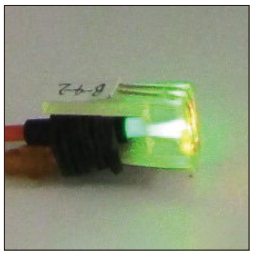

Compact and Portable Quantum Sensor Module Using Diamond NV Centers

Hiroshige DEGUCHI*, Tsukasa HAYASHI, Yoshiki NISHIBAYASHI, Minori TERAMOTO, Masanori FUJIWARA, Hiroki MORISHITA, Norikazu MIZUOCHI, and Natsuo TATSUMI

We have developed a portable measuring instrument that uses diamond nitrogen-vacancy (NV) centers. It operates on the USB 3.0 power supply of a laptop computer, consuming only 3 W of power. We use high-quality diamonds produced by Sumitomo Electric Industries, Ltd. and NHV Corporation's electron beam processing to create a sensitive NV center. The device's portability is achieved through low power consumption in both the optics and the microwave source. This is made possible by a diamond corner cube that increases the photocurrent by 2.1 times compared to planar diamonds and a microwave resonator using a λ/4 transformer and a λ/4 open stub that reduces the power by 20 dB. The sensor head is compact, measuring 5 × 10 × 20 mm, and allows for magnetic field and temperature measurements. The successful implementation of these features contributes to the use of diamond sensors in various applications.

Keywords: diamond, NV center, quantum sensor, magnetic field, temperature

1. Introduction

Among the quantum applications that are being actively researched, such as quantum computers and quantum cryptographic communications, many specific applications have been proposed for quantum sensors, which are expected to be implemented in society in the near future, with a particular focus on diamond NV centers. An NV center is a carbon atom (C) that is replaced by a pair of a nitrogen atom (N) and a vacancy in diamond, as shown in Fig. 1.

Photo 1. Single-crystal diamond

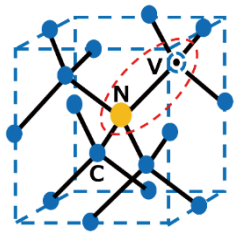

Fig. 1. Crystal structure of NV center

We create vacancies in diamond that Sumitomo Electric Industries, Ltd. (hereinafter, "Sumitomo Electric") synthesizes through the High Pressure High Temperature (HPHT) method,*1 using electron beam processing*2 of NHV Corporation (hereinafter, "NHVC"), a Sumitomo Electric Group company, or ion implantation*3 of Nissin Ion Equipment Co., Ltd., and then anneal the diamond to form an NV center.

Its fundamental properties have been measured by optical and electron spin resonance techniques,[1),(2)] and its electronic states have been studied.[3)-(5)] An NV$^-$ center has a property known as "optically detected magnetic resonance" (ODMR), in which, when exposed to green excitation light, an object emits red fluorescence whose intensity varies depending on the magnetic field and microwave resonance. The NV$^-$ center has a ground-state triplet, and a magnetic field leads to Zeeman splitting at the $m_s = \pm 1$ levels (Fig. 2). When excited by light, the electrons settle at the $m_s = 0$ level, which is the lowest, regardless of the original level; however, when a microwave at a frequency consistent with the $m_s = \pm 1$ levels is applied to the NV$^-$ center, it becomes non-luminous. By measuring this resonance frequency, the NV$^-$ center can sensitively read the surrounding magnetic and electric fields and temperature. Because of this principle of operation, improving the performance as a sensor requires an increase in the excitation light and microwave intensity, as well as the technology for highly efficient collection of fluorescence.

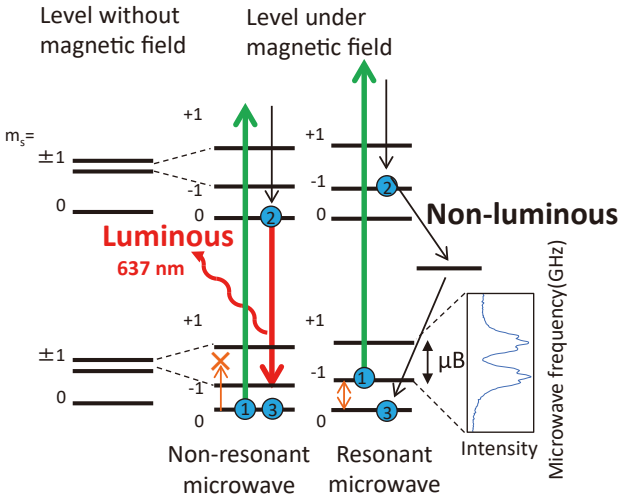

Fig. 2. Electronic state in NV$^-$ center

Furthermore, it has been shown that the spin coherence time of the NV^- center is significantly long even at room temperature,[6] and various potential applications for quantum sensors have been proposed.[7]-[10] Currently, a variety of sensor applications are under intense study, including NMR,[11]-[13] magnetocardiography and magnetoencephalography sensors,[14] in-vehicle battery sensors,[15] cellular/biological sensors,[16],[17] particle physics sensors,[18],[19] and many others.

Although the basic characteristics of NV centers have been studied on optical benches in the past, studies are now underway on their actual applications. Stürner et al. studied a coin-sized diamond sensor[20] and identified the issues of heat generated by the excitation light and the effect of the magnetic field generated by the electronic components on the magnetic field to be measured. Herbschleb et al. showed a pulsed NV sensing method over a wide dynamic range,[21] while Hatano et al. showed that the continuous-wave (CW) sensing method can be used to measure the charge and discharge currents of electric vehicle batteries over a wide dynamic range.[15] Since the microwave generation and sensor control in these papers were performed on an optical bench, size reduction is expected for automotive applications. Mariani et al. built a tabletop system for science education, which made quantum manipulation accessible.[22] However, it used an optical system similar to a microscope, and was not intended for use as a sensing system for various external magnetic fields.

For social implementation, a compact, portable sensor system is required that includes a sensor head and an excitation light source, a microwave generator, and a sensor controller. We designed this quantum sensor module so that it can be driven by a current consumption of 0.6 A and 3 W by reducing the power consumption to such a low level that the excitation light source, microwave source, and sensor control can be operated by a USB 3.0 power supply from a laptop computer. By cutting the diamond sensor into simple corner cubes, we significantly improved the efficiency of absorption, density, and collection of excitation light and fluorescence. We also describe a microwave resonator with a λ/4 open stub and a λ/4 transformer reducing the power consumption of the microwave source.[23]

2. Power Consumption Reduction Technology

2-1 Reduction of excitation light source power consumption

Since the theoretical formula for the sensitivity η of a diamond magnetic sensor[7] can be simplified using the proportional symbol and is expressed by:

$$\eta \propto \frac{1}{qC\sqrt{N_{NV}T_2^*}} \quad \cdots\cdots (1)$$

(where q is the quantum efficiency/light collection efficiency, C is the fluorescence contrast, N_{NV} is the number of NV centers, and T_2* is the spin coherent time), the sensitivity improves proportionally as the quantum efficiency/light collection efficiency, q, improves. Furthermore, since the number of NV centers excited, N_{NV}, increases in proportion to the efficiency of excitation light absorption, the greater the number, the better the sensitivity. The cutting of the diamond into corner cubes (Photo 2), which improves these properties, is described below.

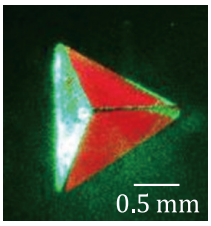

Photo 2. External view of corner cube diamond

(1) Effects of improving fluorescence collection efficiency

Diamonds appear to shine when they are brilliant-cut as gemstones; however, their simple flat or wafer-like shape is not suitable for the excitation and fluorescence detection of NV centers. In the case of a flat diamond substrate, since the refractive index is 2.4, which is much higher than that of the surrounding air, only 1.1% of the fluorescence can be collected, which is emitted within ±12.0° of the front, and the remaining fluorescence cannot be extracted outside the diamond (Fig. 3 (a)) since it is not reflected.

On the other hand, when the diamond substrate is cut into corner cubes, the fluorescence is totally reflected due to the inclination of the faces other than the face from which the fluorescence is extracted (the "extraction face"), and the light path perpendicular to the extraction face can be increased. First, there are three light paths along which the fluorescence is reflected once on one of the three sides of the corner cubes, and is directed forward (Fig. 4 (C)). Next, there are three light paths along which the fluorescence is reflected once on each of the two faces, and is directed forward (Fig. 4 (D)). In addition, there is one light path along which the fluorescence toward the opposite side

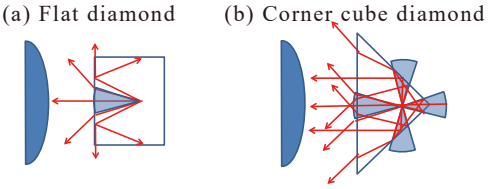

Fig. 3. Variation of light collection due to different diamond substrate geometries

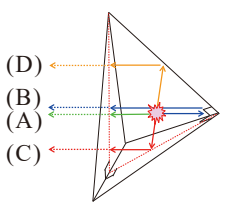

Fig. 4. Light paths of fluorescence in corner cube diamond

to the extraction face is reflected once on each of the three faces, and is directed forward (Fig. 4 (B)). In total, the fluorescence emitted at ±12.0° along a maximum of 1 + 3 + 3 + 1 = 8 light paths can be collected, improving the fluorescence collection efficiency by up to 8.8%.

(2) Effects of improving excitation light absorption efficiency and power density

In the case of a flat diamond substrate, the excitation light incident perpendicular to the plane of the diamond substrate escapes through the back face, and the light path length remains at the thickness of the substrate, d. On the other hand, in the case of a diamond substrate that is cut into corner cubes, the excitation light incident perpendicular to the bottom face has the function of total reflection, where the light is reflected once on each of the three oblique faces and returns in the direction of incidence (Fig. 5 (b)). This increases the light path length to twice that of a flat diamond and doubles the number of NV centers excited, N_{NV}, thereby doubling the excitation light absorption efficiency (if the absorption in the middle of the path is small). A comparison of the effect of improving the excitation light absorption efficiency is shown (Fig. 5).

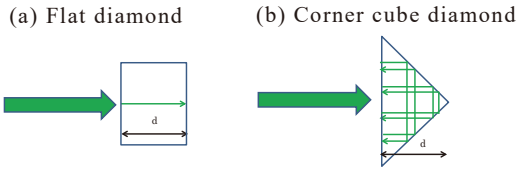

Fig. 5. Variation of excitation light path length due to different diamond substrate geometries

Assume that the power density of the excitation light is 1. In the case of a flat diamond substrate, the power density remains at 1 because only the excitation light from the front reaches the NV center. In the case of a diamond substrate that is cut into corner cubes, since the excitation light follows the reverse paths of Fig. 4, there are three paths along which the light reaches the NV center after being reflected once on one of three faces of the corner cubes (Fig. 4 (C)), three paths along which the light reaches the NV center after being reflected once on each of the two faces (Fig. 4 (D)), and one path where the light reaches NV center after being reflected once on each of the three faces (Fig. 4 (B)). Therefore, the excitation light is applied through a total of eight (1 + 3 + 3 + 1) paths, which means that the power density of the excitation light applied on the NV center is increased by a factor of 8 (at the maximum when the absorption in the middle of each path is small and the light is fully reflected on each path).

(3) Effects of improving the sensitivity of corner cube diamond

Calculating the total value of these improvement effects, assuming that the numerical aperture (NA) of the optical system (optical fiber and objective lens) that collects fluorescence is 0.5, that the absorption in the middle of each path is small, and that the optical fiber core or objective lens is sufficiently larger than the diamond substrate, substituting the light collection efficiency, q, as 8 (times) and the excitation light absorption efficiency, N_{NV}, as 2 (times) into the aforementioned theoretical formula for sensitivity yields the maximum expected sensitivity improvement of $8 \times \sqrt{2} \approx 11$ times.

(4) Comparison experiment

We compared the amount of fluorescence measured from the diamond substrate between a flat diamond substrate and a diamond substrate cut into corner cubes. All the samples in this paper were Ib-type diamonds containing nitrogen, subjected to electron beam processing at 3 MeV and 1×10^{18} cm^{-2} at NHVC, and annealed for one hour at 900°C in a vacuum. The dimensions of the corner cubes were 1.3 mm on the oblique faces and 1.7 mm on the bottom face. For both samples, a multi-mode optical fiber with a core diameter of φ400 μm and an NA of 0.5 was placed at the end and connected to a photodiode. The excitation light had a wavelength of 515 nm and an intensity of 3 mW at the fiber end. A comparison in terms of fluorescence photocurrent showed 610 nA for the flat diamond substrate and 1,300 nA for the diamond substrate cut into corner cubes, enabling data acquisition with a good signal-to-noise ratio even with low-power laser diodes.

The discrepancy between the value obtained from the experiment (2.1 times) and the theoretical value (11 times) shown in 2-1 (3) was due to the fact that the bottom face of the diamond (1.7 mm) was large relative to the core diameter of the optical fiber used in the experiment (φ400 μm), and thus the optical fiber core only covers about 1/10 of the diamond's bottom face, causing the light reflected on the sides of the diamond not to enter the optical fiber and to leak out. This experiment revealed that optimizing the core diameter of the optical fiber and the size of the diamond, as well as the processing and handling of diamonds with one side of less than 1 mm, were issues to be addressed.

2-2 Reduction of microwave source power consumption

(1) Effects of increasing microwave current

For strong magnetic resonance of the NV center, the magnetic field of the microwave must be strong. To achieve this, the microwave current must be increased. The current I in a high-frequency circuit with an output of P (W) and a characteristic impedance of Z (Ω) is expressed by

$$I = 2 \times \sqrt{P/Z}\, A_{rms} \quad \cdots\cdots (2)$$

and therefore the maximum value is obtained when the impedance of the load is 0 Ω. Therefore, the characteristic impedance of the line viewed from the load to the power supply side and the short-circuit resistance of the power supply should be lowered, while keeping the load impedance close to 0 Ω.

Assume that the root of the λ/4 open stub is the reference plane. To excite series resonance by making the load impedance viewed from the reference plane to the tip close to 0 (Ω), we used a λ/4 open stub. Also, to lower the characteristic impedance of the line viewed from the reference plane to the power supply side and the short-circuit resistance of the power supply, we used a λ/4 transformer for impedance transformation.

(2) Effects of increasing the microwave magnetic field

Next, the geometry of the λ/4 open stub for strengthening the microwave magnetic field and the characteristic

impedance of the line are described. The characteristic impedance Z_0 of the line is expressed by

$$Z_0 = \sqrt{L/C}\ (\Omega) \quad \cdots\cdots (3)$$

where L is the inductance per unit length (H/m) and C is the capacitance per unit length (F/m). The inductance per unit length is the amount of magnetic flux per unit length, and is proportional to the magnetic flux density when the width of the line of the λ/4 open stub is the same.

Therefore, to strengthen the magnetic field in the λ/4 open stub, it is necessary to adopt a line geometry with a large inductance per unit length, i.e., a large characteristic impedance. In addition, in a line with a symmetrical conductor arrangement, a uniform microwave magnetic field is generated between the conductors. Due to the large characteristic impedance of the line and the symmetrical conductor arrangement, we adopted a line with parallel two-wire geometry. Based on these considerations, we constructed a microwave-intensified resonator by using a λ/4 transformer for the impedance transformation and a λ/4 open stub for the series resonance (Fig. 6).

We determined to use a microstrip line with a characteristic impedance, Z_0, of 20 Ω as the line for the λ/4 transformer, and made a prototype with copper foil tape and a polyimide sheet. We determined to use two parallel wires with a characteristic impedance, Z_0, of 200 Ω as the line for the λ/4 open stub, and made a prototype with copper wires.

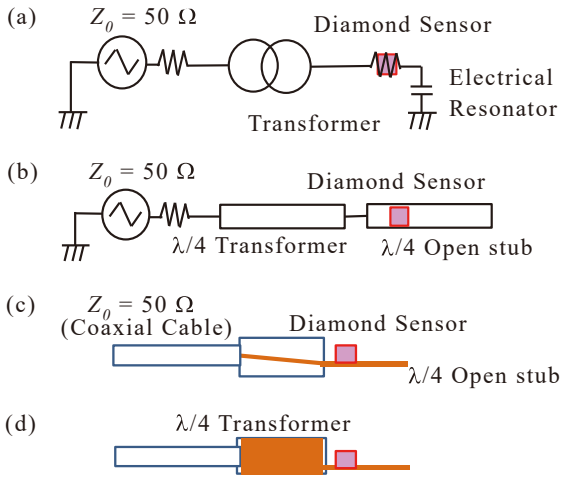

Fig. 6. Microwave resonator consisting of a λ/4 transformer and a λ/4 open stub.
(a) Concept of a resonator with a concentrated constant circuit.
(b) Concept of a resonator with distributed constant lines.
(c) Top view of a resonator consisting of a λ/4 transformer and a λ/4 open stub.
(d) Bottom view of (c)

(3) Comparison experiment

We compared this resonator to a microstrip line resonator with 50 Ω termination and a coplanar waveguide resonator with 50 Ω termination.[24] Based on the duality in electric circuits, we also compared this resonator to a λ/4 short stub resonator that was constructed by interchanging current and voltage, open and short circuits, and series and parallel resonances. The performance of the resonators was evaluated by the amount of fluorescence attenuation when the NV center was magnetically resonated, and the excitation light was set at a wavelength of 515 nm, an intensity of 15 mW, and a spot size of 60 × 120 μm. The optical system was modified from a commercially available microscope, with the LD placed in the illumination position and the PD in the eyepiece position. The direction of the microwave magnetic field was either [100] or [010] relative to the substrate [100]. No DC bias magnetic field was applied and no magnetic shielding was applied. The characteristics of the resonators were evaluated with a vector network analyzer (NanoVNA). The results of this comparison experiment are shown in Fig. 7 and Photo 3.

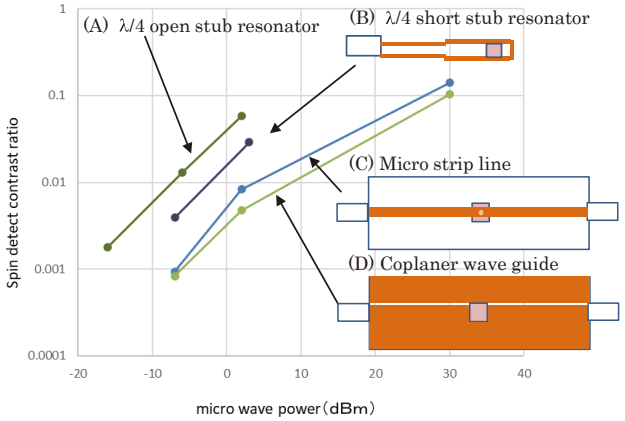

Fig. 7. Relationship between the spin detection contrast ratio and microwave power for resonators of different

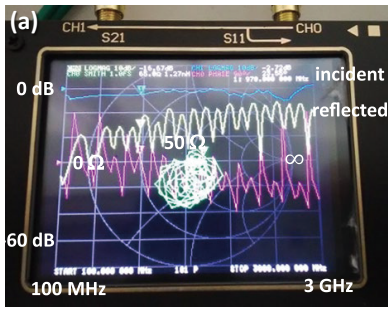

(a) 50 Ω coplaner wave guide (50 Ω termination)

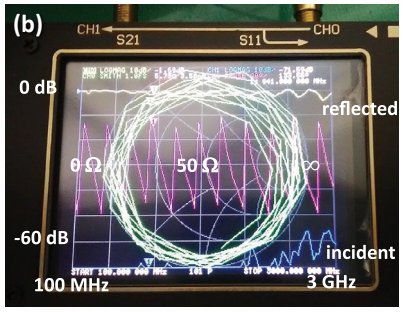

(b) λ/4 open stub resonator

Photo 3. Smith chart of resonators of different geometries

As shown in Fig. 7, the microwave resonator consisting of a λ/4 transformer and a λ/4 open stub can obtain a comparable contrast ratio with a microwave output approximately 20 dB lower than that of other resonators, and was able to measure CW-ODMR at less than 2 dBm. This allowed the output of the microwave oscillating IC (e.g., ADF4351 with an output -4 to 5 dBm) to be used without amplification, thereby reducing power consumption.

When the performance of these resonators was measured with a vector network analyzer, in a coplanar waveguide resonator with 50 Ω termination, the transmission S21 parameter was close to 1 over a wide range of 100 MHz to 3 GHz, and the Smith chart showed that it stayed near 50 Ω. The microwave resonator consisting of a λ/4 transformer and a λ/4 open stub had a reflection S11 parameter close to 1, and the Smith chart showed that it was not close to 50 Ω.

3. Diamond Sensor Module

3-1 Configuration of sensor head

The configuration of the sensor head is shown in Fig. 8 and Photo 4. Microwaves were transmitted by coaxial cable, while excitation light and fluorescence were transmitted by a single optical fiber. The aforementioned diamond substrate cut into corner cubes and the microwave resonator consisting of a λ/4 transformer and a λ/4 open stub was used.

The sensor head was a 5 mm by 10 mm by 20 mm rectangular parallelepiped, which was made compact by bending the line at two locations in the microwave resonator: at the connection between the λ/4 transformer and the λ/4 open stub, and at the center of the λ/4 open stub.

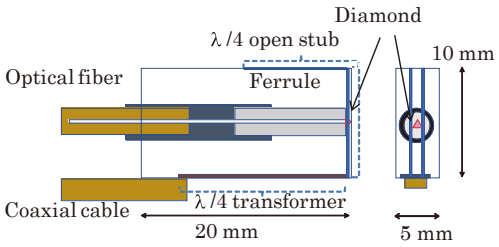

Fig. 8. Configuration of sensor head

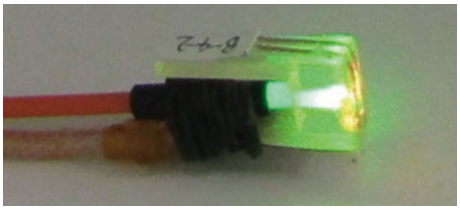

Photo 4. Sensor head

3-2 Configuration and measurement functions of control module

The control module has the functions of (1) generating excitation light, (2) generating microwaves, (3) receiving fluorescence, and (4) controlling the sensor. Table 1 shows the main components and measurement functions of the control module.

Table 1. Main components and measurement functions

Main components	
Microcomputer	Arduino Due
Excitation source laser diode	Thorlabs L515A1, wavelength 515 nm, 10 mW
Photodiode	Hamamatsu Photonics S6967 (Si series)
Optical cable	Thorlabs M126L01, core diameter 400 μmφ, NA 0.5
Microwave synthesizer	Analog Devices ADF4351 (Kit Board)
Photodetector operational amplifier	TI OPA627
DC power DC-DC converter	TDK-Lambda CC1R5-0512DF-E (±12 V output)
Measurement functions	
CW-ODMR	-1 dBm, 230 sec. (100 kHz intervals)
Temperature measurement (under zero magnetic field)	-10~70 °C, 0.7 sec. (1.4°C increments)
Fluorescence intensity measurement (fixed microwave frequency)	-1 dBm, 2.88 GHz, 0.015 sec.
Temperature measurement (under an AC magnetic field)	-40~200°C, 15 sec. (1.4°C increments)

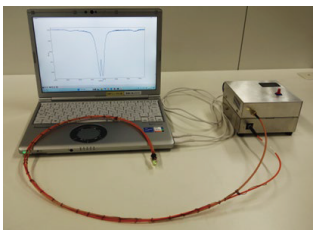

Photo 5. Sensor module connected to notebook PC

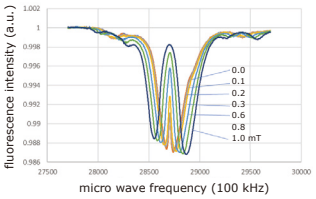

Fig. 9. CW-ODMR measurement results

3-3 Example of measurement with a sensor module

Among the measurement functions of the sensor module, an example of measurement by CW-ODMR is shown (Photo 5). In the measurement, the sensitivity of the sensor module was measured by applying a DC magnetic field in the direction of the diamond crystal [100] at 0 to 1 mT. The fluorescence intensity was 500 nA, and the fluorescence noise was 50 pArms. As shown in Fig. 9, the half-power width and the contrast ratio were 8 MHz and 1.3%, respectively. Since the magnetic field in the [100] direction was tilted 54.7° from the N-V coupling direction of [111], the magnetic rotation ratio was 28 MHz/mT × cos 54.7° = 16 MHz/mT. Since the signal-to-noise ratio of the fluorescence at this time was 50 pA / 500 nA = 0.0001, and the fluorescence was measured nine times per second, we estimated that the sensitivity was equivalent to 8 [MHz] / 16

[MHz/mT] / (0.013 / 0.0001) / $\sqrt{9}$ = 1.34 μT/$\sqrt{\text{Hz}}$. We believe that the current sensitivity can be improved by optimizing the core diameter of the optical fiber and the size of the diamond, improving the handling of diamonds with a side of less than 1 mm, and optimizing the choice of NV center concentration.

4. Conclusion

As a demonstration device for application development, we developed a quantum sensor that can be measured with a USB power supply on a tabletop. The technology of diamond substrate cutting (corner cube cutting) and microwave resonator technology (λ/4 transformer and λ/4 open stub) that enable compactness, portability, and low power consumption were introduced. We hope these diamond-related technologies will contribute to the social implementation of diamond quantum sensors.

5. Acknowledgements

Morishita would like to express his gratitude to the Division for Spintronics Research Network in the Center for Science and Innovation in Spintronics, Tohoku University. This research was partially supported by MEXT Q-LEAP (No. JPMXS0118067395) and the Center for Spintronics Research Network (Spin-RNJ).

• The names of main components in this paper are trademarks or registered trademarks of their respective companies.

Technical Terms

∗1 High Pressure High Temperature (HPHT) method: This is a method of converting raw graphite into diamond by using an ultrahigh-pressure generator to reproduce an environment in which natural diamond crystals are formed.

∗2 Electron beam processing: This is a technology for irradiating samples with high-energy electron beams, and is used for cross-linking, etc. of resin and polymer products.

∗3 Ion implantation: This is a technology for irradiating samples with high-energy ions, and is used to form doping layers in semiconductors.

References

(1) G. Davies et al., Proc. R. Soc. Lond. A. 348, 285 (1976)
(2) J. H. N. Loubser et al., Diamond Research. 11, 4 (1977)
(3) A. Lenef, S. C. Rand et al., Phys. Rev. B 53, 13441 (1996)
(4) L. J. Rogers et al., New J. Phys. 17, 013048 (2015)
(5) M. W. Doherty et al., Phys. Rev. B 85, 205203 (2012)
(6) E. D. Herbschleb et al., Nat. Commun. 10, 3766 (2019)
(7) J. M. Taylor et al., Nat. Phys. 4, 810 (2008)
(8) T. Wolf et al., Phys. Rev. X 5, 041001 (2015)
(9) C. L. Degen et al., Rev. Mod. Phys. 89, 035002 (2017)
(10) Y. Zuo et al., SUMITOMO ELECTRIC TECHNICAL REVIEW No.92, 73 (2021)
(11) S. Schmitt et al., Science 356, 832 (2017)
(12) D. Glenn et al., Nature 555, 351 (2018)
(13) E. D. Herbschleb et al., Phys.Rev.Applied 18,034058 (2022)
(14) K. Arai et al., Commun. Phys. 5, 200 (2022)
(15) Y. Hatano et al., Sci Rep. 12, 13991 (2022)
(16) R. Igarashi et al., Nano Lett. 12, 5726 (2012)
(17) B. S. Miller et al., Nature 587, 588 (2020)
(18) X. Rong et al., Nat. Commun. 9, 739 (2018)
(19) S. Chigusa et al., arXiv2302.12756 (24 Feb 2023)
(20) F. M. Stürner et al., Diam. Relat. Mater. 93, 59 (2019)
(21) E. D. Herbschleb et al., Nat. Commun. 12, 306 (2021)
(22) G. Mariani et al., AIP Adv. 12, 065321 (2022)
(23) H. Deguchi et al., Appl. Phys. Express 16, 62004 (2023)
(24) Y. Masuyama et al., Rev. Sci. Instrum. 89, 125007 (2018)

Contributors

The lead author is indicated by an asterisk (*).

H. DEGUCHI*
• Chief Senior Staff, Nissin Electric Co., Ltd.

T. HAYASHI
• Ph.D.
Chief Senior Staff, Nissin Electric Co., Ltd.

Y. NISHIBAYASHI
• Ph.D.
Senior Assistant General Manager, Advanced Materials Research Department

M. TERAMOTO
• Assistant General Manager, Sumitomo Electric Hardmetal Corp.

M. FUJIWARA
• Ph.D.
Program-Specific Researcher, Kyoto University

H. MORISHITA
• Ph.D.
Associate Professor, Tohoku University

N. MIZUOCHI
• Ph.D.
Professor, Kyoto University

N. TATSUMI
• Ph.D.
Manager, Nissin Electric Co., Ltd.

Source of reference

Deguchi Hiroshige et al., "Compact and Portable Quantum Sensor Module Using Diamond NV Centers," Nissin Electric Technical Report Vol.68, No.2, pp.63-70 (December 2023)